JACS
JOURNAL OF THE AMERICAN CHEMICAL SOCIETY
Article
pubs.acs.org/JACS

The Role of a Three Dimensionally Ordered Defect Sublattice on the Acidity of a Sulfonated Metal−Organic Framework

Jared M. Taylor,[*,†,‡] Tokutaro Komatsu,[†] Shun Dekura,[†] Kazuya Otsubo,[†,‡] Masaki Takata,[⊥,#] and Hiroshi Kitagawa[*,†,‡,§,∥]

[†]Division of Chemistry, Graduate School of Science, Kyoto University, Kitashirakawa-Oiwakecho, Sakyo-ku, Kyoto 606-8502, Japan
[‡]JST CREST, 7, Gobancho, Chiyoda-ku, Tokyo 102-0076, Japan
[§]INAMORI Frontier Research Center, Kyushu University, Motooka 744, Nishi-ku, Fukuoka 819-0395, Japan
[∥]Institute for Integrated Cell-Material Sciences (iCeMS), Kyoto University, Yoshida, Sakyo-ku, Kyoto 606-8501, Japan
[⊥]Japan Synchrotron Radiation Research Institute (JASRI), SPring-8 1-1-1 Kouto, Say-gun, Hyogo 679-5198, Japan
[#]RIKEN, SPring-8 Center, Koto 1-1-1, Sayo-cho, Sayo, Hyogo 679-5148, Japan

Supporting Information

ABSTRACT: Understanding the role that crystal imperfections or defects play on the physical properties of a solid material is important for any application. In this report, the highly unique crystal structure of the metal−organic framework (MOF) zirconium 2-sulfoterephthalate is presented. This MOF contains a large number of partially occupied ligand and metal cluster sites which directly affect the physical properties of the material. The partially occupied ligand positions give rise to a continuum of pore sizes within this highly porous MOF, supported by N_2 gas sorption and micropore analysis. Furthermore, this MOF is lined with sulfonic acid groups, implying a high proton concentration in the pore, but defective zirconium clusters are found to be effective proton trapping sites, which was investigated by a combination of AC impedance analysis to measure the proton conductivity and DFT calculations to determine the solvation energies of the protons in the pore. Based on the calculations, methods to control the pK_a of the clusters and improve the conductivity by saturating the zirconium clusters with strong acids were utilized, and a 5-fold increase in proton conductivity was achieved using these methods. High proton conductivity of 5.62×10^{-3} S cm^{-1} at 95% relative humidity and 65 °C could be achieved, with little change down to 40% relative humidity at room temperature.

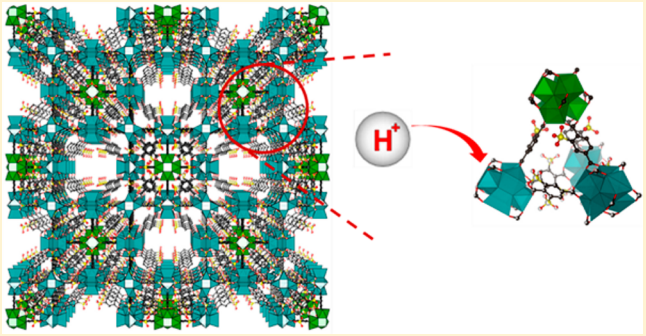

INTRODUCTION

Defects in solid-state materials have an unequivocal role on the physical properties of the solid. Intrinsic, extrinsic, or nonstoichiometric defects can give rise to a large range of magnetic, electronic, or optical properties, and by controlling the defect composition these properties can be tuned and optimized.[1] One class of solid materials where an understanding of the role of defects still remains unclear is metal−organic frameworks (MOFs). MOFs are crystalline materials composed of cationic metals or metal clusters which are bridged through organic ligands into infinite two- or three-dimensional lattices. The importance of MOFs arises from the highly tunable hybrid metal−organic nature of the material, giving rise to a huge variety of structures[2] and a number of applications, including gas storage and separation,[3] catalysis,[4] and ionic conductivity.[5] It has come to light recently that defects can occur naturally in some MOF materials, and these defects have been shown to affect the stability, catalytic, or gas storage properties of the MOF.[6] Defects in MOFs make sense from an entropic standpoint, and these recent reports bring to light the fact that the crystal structures reported for many MOFs may not fully relate to the physical properties of the material. Kinds of extrinsic defects can also be created by partial ligand replacement or metal ion replacement,[7] and the surfaces can be altered by addition of surfactants.[8] Moreover, by careful selection of additives in the synthesis, bridging ligands can be replaced with nonbridging ligands, providing a method to fine-tune the sorption or catalytic properties of the MOF by addition of defects, without altering the overall crystal structure.[9] A better understanding of the role that these defects play on the physical properties is of key importance for fine-tuning MOFs for desired applications.

Recently, we have been interested in how defects can affect the proton conducting properties of MOFs. MOFs have gained significant popularity as proton conductors owing to their highly designable nature, with potential application as novel electrolytes for low and medium temperature hydrogen fuel

Received: July 13, 2015
Published: August 24, 2015

DOI: 10.1021/jacs.5b07267
J. Am. Chem. Soc. 2015, 137, 11498−11506

cells. The pores of the MOF can be functionalized with an acidic proton source such as a phosphonic or carboxylic acid, and solvent included within the pores provides a pathway for facile proton transport, some even at temperatures above 100 °C.[10] To date, high conductivity in the range of 10^{-2} S cm^{-1} has been demonstrated for hydrated MOFs,[11] but discussions about the nature of the proton conductivity focus mainly on features revealed by the crystal structures. The roles of defects and crystal surfaces have been given little regard, even though they may have a strong influence on their conductive behavior. For example, surface conductivity has been suggested to have a major contribution to the total conductivity for some MOF materials,[12] and we have shown recently that the introduction of defects into the zirconium terephthalate UiO-66 can significantly enhance proton mobility.[13] These reports indicate that defects can have a major contribution to the conductive behavior of the MOF, but more understanding is needed in order to further optimize these materials for applications as proton conductors.

In order to gain further insight into the role defects may play in the overall conductivity, we wished to investigate an acid functionalized MOF as they typically show the highest levels of conductivity, likely due to high charge carrier concentration. These MOFs have a high density of acidic protons within their pores, but are often rather dense structures. The high density positively affects the proton carrier concentration, as the pores are lined with many acidic protons, but tends to leave restricted pathways for proton diffusion through confined solvent. As the conductivity is a product of the charge carrier concentration, charge carrier mobility, and charge, simultaneous enhancement of the carrier concentration and mobility will lead to enhancement of the conductivity. The introduction of ligand defects into an acid functionalized MOF is an optimal route to achieve this; ligand defects would slightly reduce the carrier concentration by removal of the acid functionalized ligands, but the enhanced proton mobility would likely outweigh this reduction, leading to enhanced conductivity. For this, we wanted to investigate a sulfonated MOF material, as pores lined with sulfonic acid groups should provide a high number of mobile protons due to the low pK_a of the acid.[14] There have been some reports of sulfonate functionalized MOFs recently,[11c,15] but one material stood out as a good candidate to test this hypothesis: zirconium 2-sulfoterephthalate. This crystalline material was reported to have activity as an acid catalyst, suggesting mobile protons in the pore, but no structure was reported beyond having hexanuclear zirconium clusters.[16] This was an ideal candidate as it is a zirconium-based MOF, which typically show good stability to water and heat.[17] Furthermore, defects may be easily introduced into zirconium MOFs by the use of additives during synthesis,[9e,f,18] suggesting that this may be a method to tune the proton conductivity in this MOF.

We set out to determine the structure of zirconium 2-sulfoterephthalate MOF and enhance the conductivity by defect control. What we found was a unique, highly porous MOF with an inherently defective structure containing a large number of partially occupied ligand and zirconium centers within the lattice. These defective sites have consequences on both the porosity and proton conductivity of this MOF, creating a continuum of pore sizes and greatly affecting the surface properties of the pores. Herein we present the role of these defects using a combination of gas sorption analysis, AC impedance analysis, and DFT calculations on model zirconium clusters, and present methods to control the pK_a and enhance the conductivity based on DFT proton transfer energy calculations on defective cluster models.

RESULTS AND DISCUSSION

The sulfonated zirconium terephthalate (**1**) was synthesized using a slight modification of the previously reported synthetic procedure,[16] whereby H^+ exchange on the sodium 2-sulfoterephthalic acid was performed prior to reaction with $ZrCl_4$. To ensure complete removal of residual soluble byproducts after synthesis, **1** was boiled in fresh ultrapure water and subsequently washed and soaked at least four more times in fresh ultrapure water. After washing, the powder was dried on cellulose filter paper in air, and remained stable (by PXRD) for greater than one year when stored under humid conditions greater than ∼40% relative humidity (RH). From a combination of ICP-AES and CHN analysis, an overall formula of $Zr_6O_4(OH)_8L_{4.2}{\cdot}xH_2O$ was determined (Zr/S = 1.43) assuming the sulfonate groups remain protonated, which agrees fairly well with the Zr/S of 1.5 reported previously. By thermogravimetric analysis (TGA) (Figure S1), a two step mass loss is observed, with 44 wt % loss between room temperature and 100 °C, likely corresponding to included water, and a second decomposition step beginning at 350 °C. After drying in air, **1** was measured by powder X-ray diffraction (PXRD), and was indexed using TOPAS software[19] to a cubic $Im\bar{3}$ space group with a = 41.49 Å.

For full structural analysis, indexing and structural refinement of **1** was performed using PXRD data collected in the BL02B2 beamline at SPring-8, Japan (Figure 1) (full refinement details

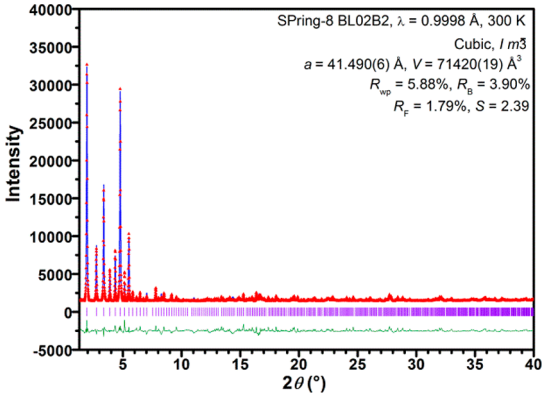

Figure 1. Rietveld plot of **1** (a) with observed (blue), calculated (red), and difference (green) curves. Indexing and refinement details inset.

in the Supporting Information). Using this data, **1** was indexed to a cubic $Im\bar{3}$ space group with a = 41.490(6) Å at 300(2) K, which is roughly double the length of the related zirconium terephthalate UiO-66 cell constant (a = 20.7004(2) Å, $Fm\bar{3}m$),[20] suggesting that the two structures should be related. UiO-66 consists of hexanuclear zirconium oxy-hydroxide clusters ($Zr_6O_4(OH)_4(R\text{-}CO_2)_{12}$) in a face-centered arrangement in the unit cell. In UiO-66, these clusters, considered from an octahedral arrangement, have 6 Zr atoms situated at the corners, 8 μ^3-O/OH in the faces, and 12 carboxylate groups which bridge two Zr centers each along the 12 edges of the octahedron. The clusters connect to 12 neighboring clusters through the linear ligand forming adjoining octahedral and tetrahedral-shaped pores. **1** can be considered to have related hexanuclear Zr clusters, but the unit cell doubling arises because

DOI: 10.1021/jacs.5b07267
J. Am. Chem. Soc. 2015, 137, 11498−11506

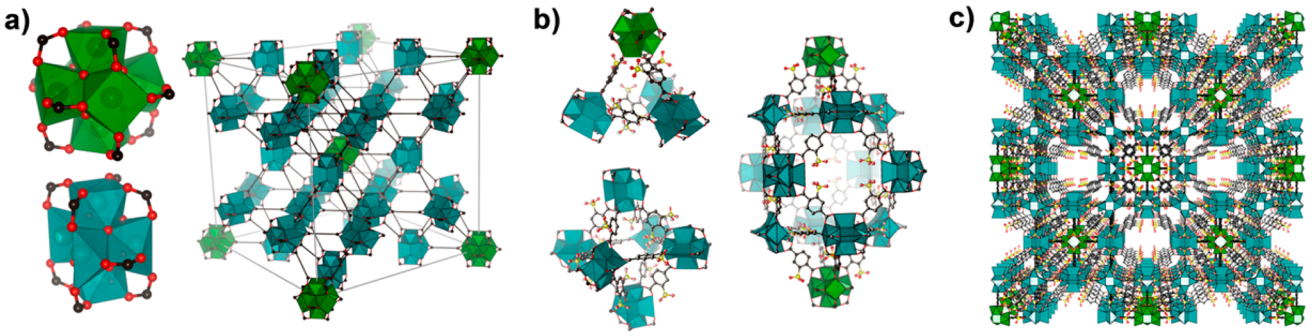

Figure 2. (a) Representations of the zirconium clusters in **1**, and their connectivity within the unit cell; the 12-connected clusters (green polyhedra) and 9-connected clusters (teal polyhedra) are differentiated. (b) Tetrahedral (top left), octahedral (bottom left), and large pore (right) within **1**. (c) View along the *a*-axis of 2 × 2 × 2 cubic cells of **1** showing the large continuous pores. C, black; O, red; S, yellow; Zr, green and teal polyhedra.

there are "vacant" cluster sites (along with ligands protruding from these clusters) equatorially at six of the eight corners of the UiO-66 unit cell (Figure 2a). These vacant cluster sites are the reason for the unit cell doubling and the body-centering of **1**, as the faces and edges of the doubled unit cell have no Zr clusters. There are 12-connected Zr clusters in the body centered positions of the unit cell which are analogous to those in UiO-66, connecting to 12 clusters centered at the (1/4, 1/4, 0) position and symmetry related sites through ordered 2-sulfoterephthalate ligands. The clusters at the (1/4, 1/4, 0) position on the other hand are only 9-connected due to the "vacant" sites at the faces and along the edges of the unit cell. These clusters are connected to one 12-connected cluster via one unique ligand and eight symmetry related 9-connected clusters via two other crystallographically unique ligands, one ordered and one with sulfonate groups disordered over two sites. This connectivity leads to three types of pores in **1**, ∼0.5 nm diameter tetrahedral pores with sulfonates occupying the pore windows, ∼0.6 nm diameter octahedral pores with disordered sulfonates partially occupying the pore space, and ∼1.2 × 2.5 nm large pores which results from the vacant cluster sites (Figure 2b). The large pores are connected through ∼0.6 × 1.3 nm rectangular windows, forming continuous pores along the *a*, *b*, and *c* axes (Figure 2c).

As stated previously, the Zr/S ratio for this material was found to be 1.43 by ICP analysis and 1.5 in the previous report. If all of the atomic sites in the determined structure remain fully occupied, a Zr/S ratio of 1.3 is found, which significantly differs from the experimental results and leads to large differences in relative intensity between the observed and calculated PXRD patterns. In order to account for this discrepancy, many of the atomic positions must remain partially occupied, meaning the apparent structure is composed of a variety of pore sizes and cluster types. For an optimal fit between the observed and calculated structure, as well as the observed Zr/S ratios, atoms forming the 9-connected zirconium clusters and the two unique ligands joining these clusters must be made partially occupied, while the 12-connected body-centered Zr-clusters and the symmetry related protruding ligands from this cluster remain fully occupied. The 9-connected cluster is formed from five unique Zr atoms (Zr2−Zr6), with occupancies of 0.6 for Zr2, 1 for Zr3, 0.8 for Zr4, 0.73 for both Zr5, and 0.85 for Zr6. The eight symmetry related O/OH of this cluster have occupancies of 0.8 and the nine bridging ligands have occupancies of 0.65 (×4), 0.72 (×4), and 1 (×1). This reduced occupancy gives an overall formula of $Zr_{4.71}O_{5.96}(OH)_{0.44}(R\text{-}CO_2)_{6.48}$ for this cluster (assuming sulfonate groups are not charge balancing). As a result of the reduced occupancies, the walls of the pores in **1** are also highly defective, with three of the six ligands forming the edges of the T_d pore having a reduced occupancy of 0.72, meaning the T_d pore has an average of 0.84 ligand vacancies out of 6 connecting ligands. The O_h pore has significantly more defects, with an average of 3.8 vacancies out of the 12 ligands which form the pore. Overall, this means that the pore structure of **1** is really a continuum of pore sizes based on the occupancies of the zirconium clusters and ligand connectors. This large number of partially occupied atoms is a rather unique feature, and to our knowledge has not been observed in another MOF system, although a partially occupied interconnected lattice has been reported previously.[6e] The mechanism for the formation of these unusual defects is currently unknown, but we believe it may be related to a combination of the highly acidic conditions during synthesis and the steric bulk of the sulfonate group. From the refined structure of **1**, a Zr/S ratio of 1.39 was determined, which matches fairly well with the Zr/S of 1.43 determined from ICP analysis of the sample.

Given the large unit cell size and highly porous nature of the MOF, full refinement of included solvent positions was difficult. In order to determine the positions of some of the water molecules in the pore, a combination of a simulated annealing method and maximum entropy method were utilized with EXPO2013,[21] RIETAN-FP,[22] Dysnomia,[23] and VESTA software,[24] as this method is useful for visualizing the electron density of included guest molecules in porous materials.[25] These analyses revealed significant residual electron density within the pore, and from this several water positions were tentatively identified (Figures S2 and S3). A formula of $Zr_6O_{7.24}(OH)_{0.89}L_{4.31}{\cdot}55H_2O$ was determined from the structural solution, which agrees well with the $Zr_6O_4(OH)_8L_{4.2}{\cdot}54H_2O$ formula determined by elemental analysis, but given that the solution was from Rietveld refinement of the PXRD data, the occupancies of the atoms are still somewhat variable while maintaining an acceptable R_{wp} value. The determined formula may suggest that some of the sulfonate groups on the ligand are deprotonated and charge balancing the Zr^{4+}, which would increase the OH/O ratio in the formula, but since no refinement of proton positions was possible, this remains unknown; it is possible that the occupancy of the O positions on the clusters is simply higher.

The structure determined from Rietveld refinement indicated that the pores in **1** are not well-defined due to the reduced occupancy of many atomic positions, so details about the micropore structure of the sample was necessary to support this

DOI: 10.1021/jacs.5b07267
J. Am. Chem. Soc. 2015, 137, 11498−11506

model. For this, N_2 gas sorption analysis was collected at 77 K, and Saito−Foley (SF) micropore analysis was performed on the adsorption data (Figure 3).[26] **1** remains stable in ambient

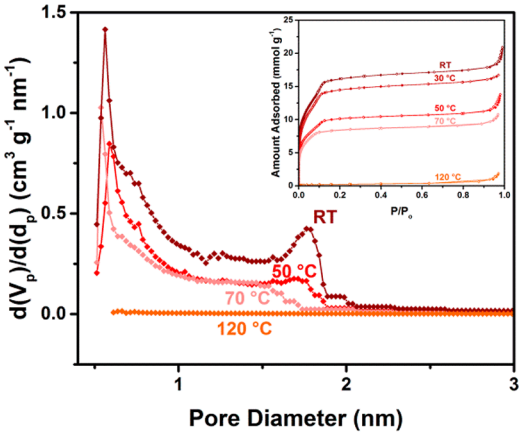

Figure 3. Saito−Foley pore size analysis of 1 under various activation conditions (given temperatures) with the N_2 gas sorption isotherms collected at 77 K (inset).

conditions for over one year, but is rather unstable to activation, decomposing rapidly upon heating with loss in crystallinity. In order to prepare the samples for gas sorption analysis, a gentle process involving solvent exchange and activation at room temperature was performed following a previously reported procedure.[27] The included water in **1** was exchanged three times each for methanol and then chloroform, after which the sample was rapidly filtered, transferred into the sample tube for gas sorption analysis and placed under vacuum for activation at room temperature. Activation was continued for 1−2 weeks, after which the N_2 gas sorption analysis was performed. Overall, N_2 adsorption occurs in a two step process between 10^{-6} − 0.15 P/P_o, with saturation of 16.9 mmol/g at 0.5 P/P_0, followed by some capillary condensation at 0.92 P/P_0. The BET surface area was calculated to be 1187 m^2/g, showing that this structure is indeed highly porous, as indicated by the crystal structure. Water sorption analysis was performed at 295 K following the N_2 sorption analysis (Figure 4), and a two step uptake was observed, with saturation at ∼50% relative humidity (RH) and a total uptake of 19.7 mmol/g at 96.1% RH; hysteresis was

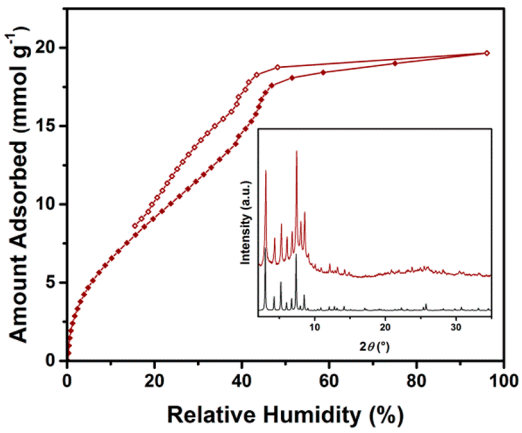

Figure 4. Water vapor adsorption (filled diamonds) and desorption (open diamonds) of 1 collected at 295 K with the post adsorption PXRD pattern (red) and simulated pattern (black) inset.

observed upon desorption. The sample remained crystalline by PXRD after both sorption measurements (Figure 4, inset). The shape of the N_2 isotherm suggests the existence of two well-defined pores in the sample, and SF micropore analysis was performed to determine the micropore size distribution and volume. From SF analysis, the total micropore volume was found to be 0.69 cm^3/g. It is clear that there are three well-defined pores in the sample, with peaks at 0.59, 0.73, and 1.71 nm, which likely correspond to the tetrahedral, octahedral, and large pores, respectively, with significant overlap between the 0.59 and 0.73 nm peaks. Furthermore, the peaks at 0.73 and 1.71 nm are rather broad, and there is a range of pore size distributions between them. This data corroborates the partial occupancies of ligands observed in the crystal structure, as this would result in the large range of pore sizes observed in the SF data. The large pore sizes with highly defective connectors may also explain why the sample is so prone to losing crystallinity upon heating, as rapid thermal fluctuations or rapid localized pressure changes may easily result in pore collapse due to the reduced connectivity of the framework.

To test the stability of the sample to heating, activation of separate batches of **1** were also performed at 30, 50, 70, and 120 °C for 24 h each under vacuum, and N_2 gas sorption analysis was performed (Figure 3, inset). Significant losses in porosity were observed by increasing the activation temperature, with total uptake reduced by 10.3%, 37.5%, 47.0%, and 97.9% at 30, 50, 70, and 120 °C activation respectively, from the 16.9 mmol/g uptake after room temperature activation. SF micropore analysis of this data (Figure 3) suggests that the larger 1.71 nm pores collapse under mild conditions, with some loss at 50 °C and complete loss at 70 °C activation. The 0.73 nm peak is also significantly reduced at 70 °C, and total micropore collapse is observed at 120 °C. This data also supports that the most defective and largest pores are the least stable, as there are a higher percentage of ligand defects observed for the O_h and large pores compared with the T_d pores. PXRD patterns collected after activation at higher temperatures show significant loss of crystallinity at 70 °C and nearly total amorphization at 120 °C (Figure S5).

Based on the structure of **1**, it appears that it should make for a fantastic proton conductor, as it combines a number of important structural features which promote high proton conductivity: First, the structure is lined with a significant number of highly acidic sulfonic acid groups (1.26×10^{21} cm^{-3} based on the unit cell volume), which is comparable to benchmark sulfonated polymeric electrolytes.[28] Second, **1** contains large, open, hydrated, three-dimensionally interconnected pores, which suggests that any protons should be highly mobile within the framework structure. And finally, the ligand defects which result from the reduced ligand occupancy should further promote high charge mobility as the pores are more open than the crystal structure would suggest. As such, pseudo-four-probe AC impedance analysis was performed on pelletized samples of **1** in order to determine the bulk proton conductivity. After pelletization, gold electrodes were affixed to the surface of the pellets and the samples were equilibrated under controlled temperature and humidity. Variable temperature impedance analysis was performed on two sample batches of **1** at 95% RH between 15 and 65 °C in order to determine the activation energy (E_a) for proton transport (Figure 5). For each sample, the AC frequency was cycled from 10^7 Hz to 1 Hz, and two distinct semicircles were observed, which indicates separate grain interior and grain boundary contributions

DOI: 10.1021/jacs.5b07267
J. Am. Chem. Soc. 2015, 137, 11498−11506

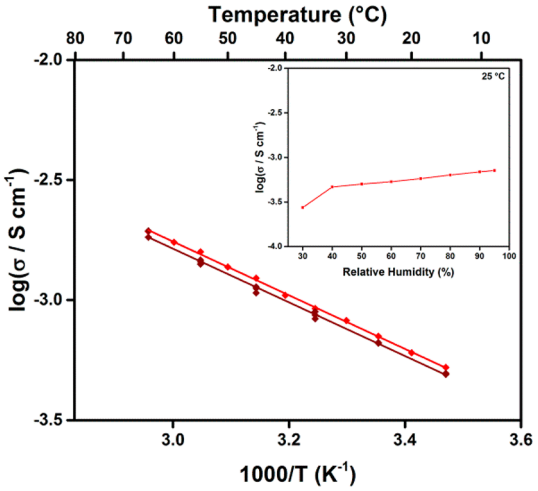

Figure 5. Variable temperature conductivity of two separate samples batches of **1** collected at 95% RH which show linear Arrhenius behavior. The variable humidity conductivity is inset.

(Figure S6). The resistance was found by fitting parallel RC elements to the first semicircle (Figures S7–S11), and the conductivity was determined from this using the pellet dimensions. At 65 °C, the conductivity of both samples was determined to be comparable at 1.93×10^{-3} and 1.82×10^{-3} S/cm, with low activation energies of 0.25 eV for both samples, which suggests proton transport by a Grotthuss-type mechanism.[29] The comparable values for conductivity for both samples show that the result is reproducible. But while these values of conductivity are good, they are roughly 2 orders of magnitude lower than the benchmark polymeric electrolytes, and about 1 order of magnitude lower than many other MOFs under similar measurement conditions. The highly porous nature of the MOF should promote high proton mobility, so the reduced conductivity likely stems from a reduction in the H^+ concentration within the pore. This suggests that there is some feature in the MOF which causes the sulfonate groups to have reduced acidity.

Variable humidity impedance analysis was also performed on **1** (Figure 5, inset), and the material showed very little desorption of water down to ~40% RH, suggesting it might have good conductivity at lower humidity. The conductivity was measured from 95% RH to 30% RH at 25 °C, and remarkably there was little change in the conductivity down to 30% RH, with the conductivity decreasing from 7.15×10^{-4} S/cm at 95% RH to 4.66×10^{-4} S/cm at 40% RH and 30% RH to 2.75×10^{-4} S/cm. This is remarkable considering that for most hydrated MOF proton conductors the conductivity typically drops by orders of magnitude upon decreasing relative humidity, even between 95% RH to 80% RH. The high conductivity even at low relative humidity highlights the hydrophilic nature of **1**, and correlates well with the saturation plateau and hysteresis observed in the water desorption

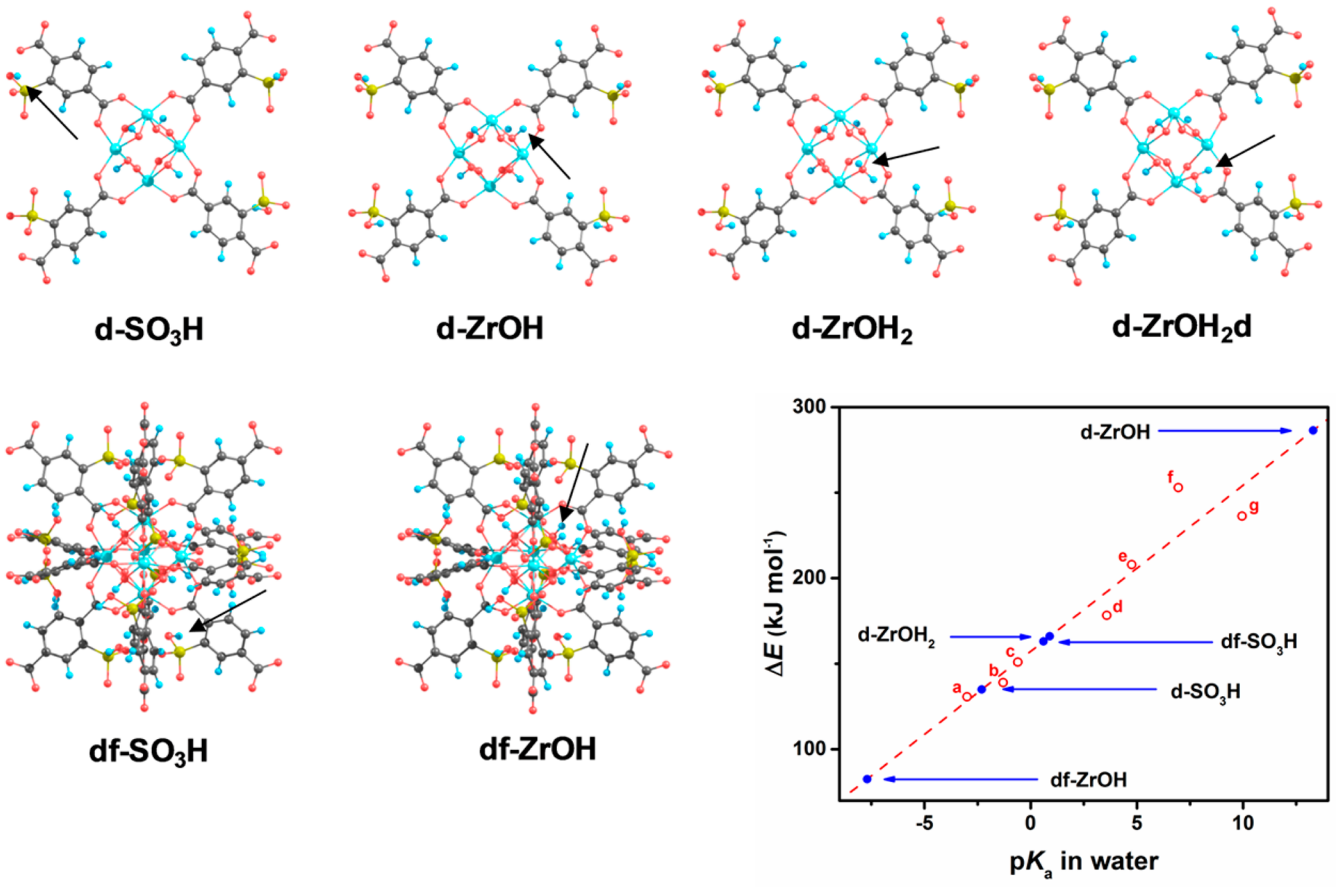

Figure 6. Structural models of the clusters used for DFT calculations (C, black; H, blue; O, red; S, dark yellow; Zr, teal) and their estimated pK_a's in water in comparison to known acids (a, H_2SO_4; b, HNO_3; c, CH_3SO_3H; d, H_2CO_3; e, CH_3COOH; f, imidazole; g, phenol). The positions of the acidic protons are indicated by the arrows.

DOI: 10.1021/jacs.5b07267
J. Am. Chem. Soc. 2015, 137, 11498–11506

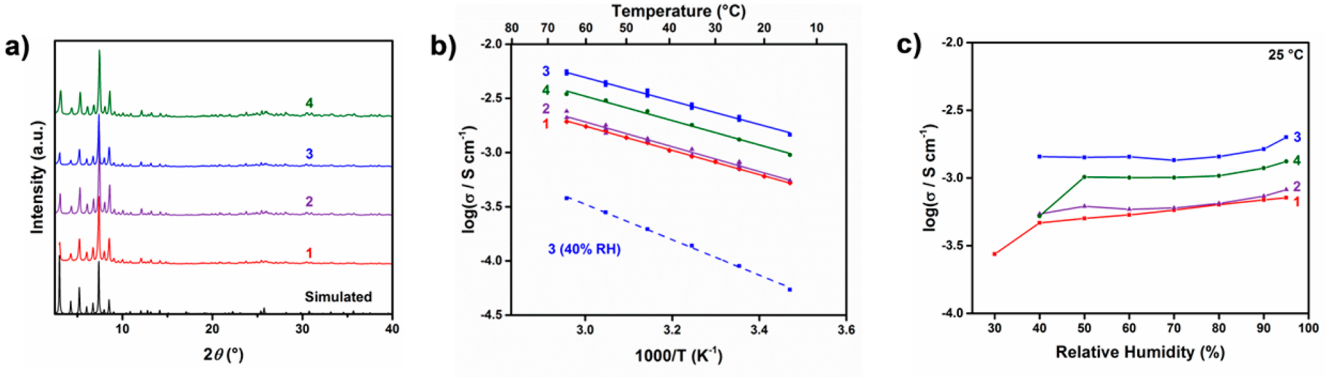

Figure 7. (a) PXRD charts of samples **1**−**4**. (b) Variable temperature conductivity of samples **1**−**4** collected at 95% RH (solid lines) and 40% RH (dashed line) showing linear Arrhenius behavior. (c) Variable humidity conductivity at 25 °C of samples **1**−**4**.

isotherm. The high conductivity at low % RH makes **1** among the highest proton conducting MOFs under reduced humidity.

While the conductivity is high at low relative humidity, the unexpectedly low conductivity at high relative humidity suggests that the proton carried by sulfonic acid groups within **1** may be trapped in some way, significantly lowering the charge carrier concentration. This is remarkable, considering the highly acidic synthetic conditions (pH < 1) with excess ligand used during synthesis, and indicates that the zirconium oxohydroxy clusters may act as proton trapping sites. To understand this behavior, density functional theory calculations were performed on model structures. The model crystal structure was constructed by adding hydrogens and sulfonic acid groups to a defect free framework from the previously reported UiO-66 crystal structure using Materials Studio 7.0 software. Defective frameworks were constructed by omitting ligands and Zr^{4+} from this model. The models were optimized as a periodic structure using the molecular mechanics simulator Forcite with a Universal Force Field[30] incorporated within Materials Studio. The acidity was evaluated as the energy required for proton transfer from the model cluster HA to H_2O in water:

$$HA_{(aq)} + H_2O + \Delta E = A^-_{(aq)} + H_3O^+_{(aq)}$$

The five model structures for HA are df-SO_3H, df-ZrOH, d-SO_3H, d-ZrOH, and d-$ZrOH_2$ (Figure 6), where df is defect free, d is defective, and formula after indicates the position of the acidic H^+. The two model structures for A^- are df-SO_3^- and d-SO_3^-. The defect free cluster is the typical $Zr_6O_4(OH)_4(R\text{-}CO_2)_{12}$ cluster, while the defective cluster was constructed from this by omitting two Zr^{4+} and four ligands, giving a $Zr_4O_4(OH)_4(R\text{-}CO_2)_4$ cluster (Figure S12). While many other model defective clusters are possible based on the crystal structure of **1**, we were unable to examine the full gamut of cluster types due to limited computational resources. For single point energy calculations on the solvated models, we employed density functional theory (B3PW91 hybrid functional) implemented in the Firefly QC package[31] which is partially based on the GAMESS (US)[32] source code. For Zr, the Stuttgart RSC 1997 ECP basis set was applied, while for the other elements 6-31D(d) basis sets were used. To represent negatively charged states, diffuse functions were added to the basis functions for oxygen and sulfur. To improve the SCF convergence, components that gave overlap-matrix eigenvalues less than 4×10^{-6} were omitted from the basis function. The solvation energy was corrected with the polarizable continuum model.

The ΔE's of common acids were calculated (Table S3), and are in a roughly linear relationship with their experimental pK_a in water (Figure 5),[38] so accordingly, the pK_a of the model clusters can be estimated from the calculated ΔE's using the equation:

$$pK_a = 0.103\Delta E - 16.2$$

From this, the estimated pK_a of the sulfonic acid group in d-SO_3H is −2.3, which is comparable to strong acids such as nitric and sulfuric acid. In comparison, the sulfonic acid group in df-SO_3H shows weaker acidity (pK_a = 0.6), but is still comparable to, for example, CH_3SO_3H. Therefore, if there were no other factors, the introduction of sulfonic acid groups into **1** would result in a high concentration of H^+ in the pores. However, from our models, released protons are found to be trapped at the defective cluster sites, forming a more stable structure than d-SO_3H. The μ_2-oxide in the defect containing cluster can act as a strong proton trapping site (d-ZrOH), since the estimated pK_a of 13.3 is comparable to alcohols. The μ_2-hydroxyl (d-$ZrOH_2$) on the other hand does not strongly trap protons (pK_a = 0.9), but interestingly can be further stabilized by breaking one bond between the μ_2-water and Zr^{4+} (d-$ZrOH_2$d), resulting in a structure that is more stable by 115.7 kJ/mol (Scheme S1). Our calculations do not indicate the energy barrier of this process, but it is safe to say it is an irreversible process. This stabilization by coordination bond breaking may be the source of instability to activation in this MOF, as loss of bridging water would likely lead to collapse of the cluster. Trapping of a proton at the oxide in the defect free cluster (df-ZrOH) results in a pK_a of −7.7, which is far smaller than df-SO_3H, suggesting that the defect free cluster does not act as a H^+ trapping site. This strongly indicates that the partially occupied clusters within **1** regulate the pore acidity by significantly lowering the charge carrier concentration, acting as an intrinsic buffering system. This result has implications not only for proton conductivity, but any process involving protons within the MOF, for example, acid catalysis. This also suggests that cluster defects causing exposed hydroxyl/oxides in related Zr^{4+} based MOFs may be a source of instability to strong acids.

The computational results indicated that the proton conductivity of **1** could be improved if the proton trapping nature of the defective sites could be saturated by the addition of stronger acids into the synthesis, thereby causing partial protonation of the sulfonate groups and reducing the pK_a of the MOF. To test this hypothesis, three more samples were prepared in the presence of excess acidic additives. For two

DOI: 10.1021/jacs.5b07267
J. Am. Chem. Soc. 2015, 137, 11498−11506

samples, an excess of a secondary acid was added during synthesis: acetic acid (**2**) and sulfoacetic acid (**3**). For the third sample, **1** was soaked in 0.1 M $H_2SO_{4(aq)}$ overnight postsynthetically (**4**). Sulfoacetic acid and sulfuric acid were chosen because it has previously been demonstrated that sulfuric acid can bind to related zirconium clusters and strongly increase the acidity of the MOF.[27] All of the treated samples were washed extensively and soaked multiple times in ultrapure water to ensure the removal of any residual acid. The carboxylic acid additives were added during synthesis with the hope that they may also fill some of the defective zirconium cluster sites and increase the stability of the MOF. By ^{1}H NMR analysis of dried samples dissolved in a D_2O/D_2SO_4 solution, sample **2** contained acetate (s, 2.08 ppm) and 2-sulfoterephthalate (d, 8.50 ppm; d of d, 8.19 ppm; d, 7.69 ppm) in a 20:1 ligand to acetate ratio by integration. Sample **3** contatined sulfoacetate (s, 3.47 ppm) and a second residual peak (s 3.17 ppm), giving a 25:1 ligand to sulfoacetate ratio; the second residual peak may be a result of the partial decomposition of the sulfoacetic acid during synthesis or NMR sample preparation. Elemental analysis on the samples following treatment showed that they all have a formula of roughly $Zr_6O_4(OH)L_4{\cdot}xH_2O$, with Zr/S ratios of 1.50 for **2** and **3**, and 1.56 for **4**, and the PXRD patterns of all of the treated samples remained unchanged (Figure 7a).

N_2 gas sorption analysis was performed at 77 K on **2**–**4** after undergoing the same gentle activation procedure as **1**, and each showed high porosity, and the same shape of isotherm as **1**, suggesting similar micropore structure (Figure S13). There were minor variations in the total uptake, but these differences may result from residual solvent in the pores from the gentle activation procedure, rather than changes in pore structure; **3** had the greatest uptake of 19.1 mmol/g at 0.50 P/P_0. Water vapor sorption at 295 K (Figure S14) showed significant uptake of water for **3** (30.4 mmol/g at 97.9% RH) and **4** (26.9 mmol/g at 94.5% RH), but significantly reduced uptake for **2** (12.0 mmol/g at 96.8% RH); hysteresis was observed for all of the samples. The ∼50% greater uptake of water for **3** compared to **1** suggests that the pores in **1** may have slightly collapsed following the N_2 sorption. The uptake of water for **3** was 52.5 mol/mol at 0.98 P/P_o, which matches well with the 55 mol/mol determined by XRD. Post adsorption PXRD (Figure S15) showed that **2** had undergone some decomposition and structural changes, suggesting partial pore collapse, while **3** and **4** remained mostly stable, with some line broadening. The overall stability of the samples also remained unchanged with the acidic additives, being stable when hydrated, but decomposing rapidly upon heating under ambient conditions.

To test whether the acid treatment improved the proton conductivity of the samples, AC impedance analysis of pelletized powders of samples **2**–**4** was carried out (Figure 7b). The samples were equilibrated under 95% RH, and variable temperature measurements were carried out. Sample **2**, treated with the relatively weaker acetic acid, had about double the conductivity compared to **1**, with a maximum of 2.40×10^{-3} S/cm at 65 °C and the same E_a of 0.25 eV. On the other hand, samples **3** and **4**, treated with highly acidic sulfoacetic and sulfuric acid, respectively, showed significantly improved conductivity with a maximum of 5.62×10^{-3} and 3.46×10^{-3} S/cm at 95% RH, respectively, with similar activation energies of 0.24 and 0.25 eV. If the gains in conductivity are solely from increased carrier concentration, it would suggest that the acid treatment causes the carrier concentration to increase by roughly 5-fold in **3**. The nearly equivalent E_a for **1**–**4**, along with the nearly equivalent porosities indicate that the proton transport mechanism and likely diffusion coefficients remain unchanged by acid treatment. This result shows that, as indicated by the computational analysis, the treatment of the MOF with more acidic protic species results in the partial filling of proton trapping sites, thus increasing the carrier concentration within the pores.

Variable humidity measurements were also performed between 95% RH and 40% RH on samples **2**–**4**, and similar behavior to **1** was observed (Figure 7c). The conductivity of samples **2**–**4** fell slightly between 95% to 80% RH, but remained relatively constant down to 40% RH, with long equilibration times of 1 day for each point. In particular, sample **3** had a conductivity of 1.4×10^{-3} S/cm at 40% RH, which is remarkably high for the moderate %RH value, and to our knowledge the best performing hydrated MOF under such conditions. In order to measure the E_a at 40% RH, the temperature was cycled between 15 and 65 °C for **3**. Upon heating, it became clear that the high conductivity observed at 40% RH represented a metastable state of hydration, as the conductivity dropped upon increasing the temperature, reaching a value of 3.78×10^{-4} S/cm at 65 °C. Upon cooling, the conductivity again showed Arrhenius behavior, with an E_a of 0.35 eV, likely from more restricted proton mobility in **3** at 40% RH, and the MOF remained crystalline after analysis (Figure S16). Despite the drop in conductivity upon heating, the value still remains high compared to other MOF materials under the low humidity conditions. These results show that measuring conductivity as a function of relative humidity for MOF materials may require higher temperatures in order to accurately represent the equilibrium state of hydration.

CONCLUSIONS

Here we have reported a new and unique structure of a sulfonated zirconium based MOF containing an ordered defect sublattice, its proton conducting properties, and the role of the defects in controlling the acidity within the MOF. The sulfonated zirconium MOF **1** is highly porous, with a three-dimensional interconnected framework having the unique feature of many partially occupied ligand and cluster sites, which gives rise to a continuum of pore sizes. The proton conductivity of the MOF was measured, and despite being functionalized with numerous sulfonic acid groups, the carrier concentration is attenuated by the presence of the defective oxohydroxy zirconium clusters which have increased basic character compared to defect free clusters. Calculations on the charge trapping nature of the zirconium cluster suggested that acid treatment of the MOF could saturate the charge trapping sites and improve the overall conductivity, and by synthesis in the presence of sulfoacetic acid, a 5-fold improvement of the conductivity was achieved, reaching a maximum of 5.62×10^{-3} S cm^{-1} at 95% relative humidity and 65 °C. Overall, these results demonstrate that defective sites within MOFs can significantly alter the surface properties of the MOF, in this case causing large changes to the proton trapping nature of the material. These results not only are important for the application of MOFs as proton conductors, but also give insight into their stability and potential limitations as acid catalysts. Hopefully, the results presented here can be utilized for the design of more active protic MOF materials.

DOI: 10.1021/jacs.5b07267
J. Am. Chem. Soc. 2015, 137, 11498–11506

■ ASSOCIATED CONTENT

Supporting Information

The Supporting Information is available free of charge on the ACS Publications website at DOI: 10.1021/jacs.5b07267.

Synthetic and experimental details; TGA; PXRD; Cole−Cole plots and circuit fitting; sorption analysis; DFT calculation information (PDF)

Crystal structure refinement information (CIF)

■ AUTHOR INFORMATION

Corresponding Authors

*taylorjm@kuchem.kyoto-u.ac.jp.

*kitagawa@kuchem.kyoto-u.ac.jp.

Present Address

[∇]M.T.: Institute of Multidisciplinary Research for Advanced Materials, Tohoku University, Katahira 2−1−1, Aoba-ku, Sendai 980−8577, Japan.

Notes

The authors declare no competing financial interest.

■ ACKNOWLEDGMENTS

This work was partly supported by Grants-in-Aid for Scientific Research No. 20350030 and No. 23245012 from the Ministry of Education, Culture, Sports, Science and Technology of Japan. Synchrotron X-ray diffraction measurement was supported by the Japan Synchrotron Radiation Research Institute (JASRI) (Proposal No. 2014A1425).

■ REFERENCES

(1) Tilley, R. J. D. *Defects in Solids*; John Wiley & Sons Inc.: Hoboken, NJ, 2008.

(2) O'Keeffe, M.; Yaghi, O. M. *Chem. Rev.* **2012**, *112*, 675.

(3) (a) Canivet, J.; Fateeva, A.; Guo, Y.; Coasne, B.; Farrusseng, D. *Chem. Soc. Rev.* **2014**, *43*, 5594. (b) Qiu, S.; Xue, M.; Zhu, G. *Chem. Soc. Rev.* **2014**, *43*, 6116. (c) Van de Voorde, B.; Bueken, B.; Denayer, J.; De Vos, D. *Chem. Soc. Rev.* **2014**, *43*, 5766.

(4) Gao, W.-Y.; Chrzanowski, M.; Ma, S. *Chem. Soc. Rev.* **2014**, *43*, 5841.

(5) Ramaswamy, P.; Wong, N. E.; Shimizu, G. K. H. *Chem. Soc. Rev.* **2014**, *43*, 5313.

(6) (a) Ameloot, R.; Vermoortele, F.; Hofkens, J.; De Schryver, F. C.; De Vos, D. E.; Roeffaers, M. B. J. *Angew. Chem., Int. Ed.* **2013**, *52*, 401. (b) Liu, M.; Wong-Foy, A. G.; Vallery, R. S.; Frieze, W. E.; Schnobrich, J. K.; Gidley, D. W.; Matzger, A. J. *Adv. Mater.* **2010**, *22*, 1598. (c) Noei, H.; Amirjalayer, S.; Müller, M.; Zhang, X.; Schmid, R.; Muhler, M.; Fischer, R. A.; Wang, Y. *ChemCatChem* **2012**, *4*, 755. (d) Valenzano, L.; Civalleri, B.; Chavan, S.; Bordiga, S.; Nilsen, M. H.; Jakobsen, S.; Lillerud, K. P.; Lamberti, C. *Chem. Mater.* **2011**, *23*, 1700. (e) Yang, S.; Lin, X.; Lewis, W.; Suyetin, M.; Bichoutskaia, E.; Parker, J. E.; Tang, C. C.; Allan, D. R.; Rizkallah, P. J.; Hubberstey, P.; Champness, N. R.; Thomas, K. M.; Blake, A. J.; Schröder, M. *Nat. Mater.* **2012**, *11*, 710. (f) Shoaee, M.; Anderson, M. W.; Attfield, M. P. *Angew. Chem., Int. Ed.* **2008**, *47*, 8525.

(7) (a) Kim, M.; Cahill, J. F.; Su, Y.; Prather, K. A.; Cohen, S. M. *Chem. Sci.* **2012**, *3*, 126. (b) Kim, M.; Cahill, J. F.; Fei, H.; Prather, K. A.; Cohen, S. M. *J. Am. Chem. Soc.* **2012**, *134*, 18082. (c) Fei, H.; Cahill, J. F.; Prather, K. A.; Cohen, S. M. *Inorg. Chem.* **2013**, *52*, 4011. (d) Wang, L. J.; Deng, H.; Furukawa, H.; Gándara, F.; Cordova, K. E.; Peri, D.; Yaghi, O. M. *Inorg. Chem.* **2014**, *53*, 5881.

(8) (a) Choi, K. M.; Jeon, H. J.; Kang, J. K.; Yaghi, O. M. *J. Am. Chem. Soc.* **2011**, *133*, 11920. (b) Huang, X.-X.; Qiu, L.-G.; Zhang, W.; Yuan, Y.-P.; Jiang, X.; Xie, A.-J.; Shen, Y.-H.; Zhu, J.-F. *CrystEngComm* **2012**, *14*, 1613.

(9) (a) Park, J.; Wang, Z. U.; Sun, L.-B.; Chen, Y.-P.; Zhou, H.-C. *J. Am. Chem. Soc.* **2012**, *134*, 20110. (b) Fang, Z.; Dürholt, J. P.; Kauer, M.; Zhang, W.; Lochenie, C.; Jee, B.; Albada, B.; Metzler-Nolte, N.; Pöppl, A.; Weber, B.; Muhler, M.; Wang, Y.; Schmid, R.; Fischer, R. A. *J. Am. Chem. Soc.* **2014**, *136*, 9627. (c) Kozachuk, O.; Luz, I.; Llabrés i Xamena, F. X.; Noei, H.; Kauer, M.; Albada, H. B.; Bloch, E. D.; Marler, B.; Wang, Y.; Muhler, M.; Fischer, R. A. *Angew. Chem., Int. Ed.* **2014**, *53*, 7058. (d) Bueken, B.; Reinsch, H.; Reimer, N.; Stassen, I.; Vermoortele, F.; Ameloot, R.; Stock, N.; Kirschhock, C. E. A.; De Vos, D. *Chem. Commun.* **2014**, *50*, 10055. (e) Vermoortele, F.; Bueken, B.; Le Bars, G.; Van de Voorde, B.; Vandichel, M.; Houthoofd, K.; Vimont, A.; Daturi, M.; Waroquier, M.; Van Speybroeck, V.; Kirschhock, C.; De Vos, D. E. *J. Am. Chem. Soc.* **2013**, *135*, 11465. (f) Wu, H.; Chua, Y. S.; Krungleviciute, V.; Tyagi, M.; Chen, P.; Yildirim, T.; Zhou, W. *J. Am. Chem. Soc.* **2013**, *135*, 10525.

(10) (a) Okawa, H.; Sadakiyo, M.; Yamada, T.; Maesato, M.; Ohba, M.; Kitagawa, H. *J. Am. Chem. Soc.* **2013**, *135*, 2256. (b) Taylor, J. M.; Vaidhyanathan, R.; Iremonger, S. S.; Shimizu, G. K. H. *J. Am. Chem. Soc.* **2012**, *134*, 14338. (c) Begum, S.; Wang, Z.; Donnadio, A.; Costantino, F.; Casciola, M.; Valiullin, R.; Chmelik, C.; Bertmer, M.; Kärger, J.; Haase, J.; Krautscheid, H. *Chem. - Eur. J.* **2014**, *20*, 8862. (c) Bao, S.-S.; Otsubo, K.; Taylor, J. M.; Jiang, Z.; Zheng, L.-M.; Kitagawa, H. *J. Am. Chem. Soc.* **2014**, *136*, 9292. (d) Jeong, N. C.; Samanta, B.; Lee, C. Y.; Farha, O. K.; Hupp, J. T. *J. Am. Chem. Soc.* **2012**, *134*, 51. (d) Phang, W. J.; Lee, W. R.; Yoo, K.; Ryu, D. W.; Kim, B.; Hong, C. S. *Angew. Chem., Int. Ed.* **2014**, *53*, 8383. (e) Horike, S.; Kamitsubo, Y.; Inukai, M.; Fukushima, T.; Umeyama, D.; Itakura, T.; Kitagawa, S. *J. Am. Chem. Soc.* **2013**, *135*, 4612. (f) Tang, Q.; Liu, Y.; Liu, S.; He, D.; Miao, J.; Wang, X.; Yang, G.; Shi, Z.; Zheng, Z. *J. Am. Chem. Soc.* **2014**, *136*, 12444. (g) Hurd, J. A.; Vaidhyanathan, R.; Thangadurai, V.; Ratcliffe, C. I.; Moudrakovski, I. L.; Shimizu, G. K. H. *Nat. Chem.* **2009**, *1*, 705. (h) Ponomareva, V. G.; Kovalenko, K. a; Chupakhin, A. P.; Dybtsev, D. N.; Shutova, E. S.; Fedin, V. P. *J. Am. Chem. Soc.* **2012**, *134*, 15640. (i) Bureekaew, S.; Horike, S.; Higuchi, M.; Mizuno, M.; Kawamura, T.; Tanaka, D.; Yanai, N.; Kitagawa, S. *Nat. Mater.* **2009**, *8*, 831.

(11) (a) Sadakiyo, M.; Yamada, T.; Kitagawa, H. *J. Am. Chem. Soc.* **2009**, *131*, 9906. (b) Kim, S.; Dawson, K. W.; Gelfand, B. S.; Taylor, J. M.; Shimizu, G. K. H. *J. Am. Chem. Soc.* **2013**, *135*, 963. (c) Phang, W. J.; Jo, H.; Lee, W. R.; Song, J. H.; Yoo, K.; Kim, B.; Hong, C. S. *Angew. Chem., Int. Ed.* **2015**, *54*, 5142.

(12) Tominaka, S.; Cheetham, A. K. *RSC Adv.* **2014**, *4*, 54382.

(13) Taylor, J. M.; Dekura, S.; Ikeda, R.; Kitagawa, H. *Chem. Mater.* **2015**, *27*, 2286.

(14) *CRC Handbook of Chemistry and Physics*, 92nd ed.; Haynes, W. M., Ed.; CRC Press: Boca Raton, FL, 2011.

(15) (a) Lin Foo, M.; Horike, S.; Fukushima, T.; Hijikata, Y.; Kubota, Y.; Takata, M.; Kitagawa, S. *Dalton Trans.* **2012**, *41*, 13791. (b) Akiyama, G.; Matsuda, R.; Sato, H.; Takata, M.; Kitagawa, S. *Adv. Mater.* **2011**, *23*, 3294.

(16) Juan-Alcañiz, J.; Gielisse, R.; Lago, A. B.; Ramos-Fernandez, E. V.; Serra-Crespo, P.; Devic, T.; Guillou, N.; Serre, C.; Kapteijn, F.; Gascon, J. *Catal. Sci. Technol.* **2013**, *3*, 2311.

(17) DeCoste, J. B.; Peterson, G. W.; Jasuja, H.; Glover, T. G.; Huang, Y.; Walton, K. S. *J. Mater. Chem. A* **2013**, *1*, 5642.

(18) Cliffe, M. J.; Wan, W.; Zou, X.; Chater, P. a; Kleppe, A. K.; Tucker, M. G.; Wilhelm, H.; Funnell, N. P.; Coudert, F.-X.; Goodwin, A. L. *Nat. Commun.* **2014**, *5*, 4176.

(19) Bruker AXS, TOPAS V3: General profile and structure analysis software for powder diffraction data, Karlsruhe, Germany, 2005.

(20) Cavka, J. H.; Jakobsen, S.; Olsbye, U.; Guillou, N.; Lamberti, C.; Bordiga, S.; Lillerud, K. P. *J. Am. Chem. Soc.* **2008**, *130*, 13850.

(21) Altomare, A.; Cuocci, C.; Giacovazzo, C.; Moliterni, A.; Rizzi, R.; Corriero, N.; Falcicchio, A. *J. Appl. Crystallogr.* **2013**, *46*, 1231.

(22) Izumi, F.; Momma, K. *Solid State Phenom.* **2007**, *130*, 15.

(23) Momma, K.; Ikeda, T.; Belik, A. A.; Izumi, F. *Powder Diffr.* **2013**, *28*, 184.

(24) Momma, K.; Izumi, F. *J. Appl. Crystallogr.* **2011**, *44*, 1272 DOI: 10.1107/S0021889811038970.

(25) (a) Matsuda, R.; Kitaura, R.; Kitagawa, S.; Kubota, Y.; Belosludov, R. V.; Kobayashi, T. C.; Sakamoto, H.; Chiba, T.;

Takata, M.; Kawazoe, Y.; Mita, Y. *Nature* **2005**, *436*, 238. (b) Fujita, D.; Suzuki, K.; Sato, S.; Yagi-Utsumi, M.; Yamaguchi, Y.; Mizuno, N.; Kumasaka, T.; Takata, M.; Noda, M.; Uchiyama, S.; Kato, K.; Fujita, M. *Nat. Commun.* **2012**, *3*, 1093. (c) Sadakiyo, M.; Kasai, H.; Kato, K.; Takata, M.; Yamauchi, M. *J. Am. Chem. Soc.* **2014**, *136*, 1702.
(26) Saito, A.; Foley, H. C. *AIChE J.* **1991**, *37*, 429.
(27) Jiang, J.; Gándara, F.; Zhang, Y.-B.; Na, K.; Yaghi, O. M.; Klemperer, W. G. *J. Am. Chem. Soc.* **2014**, *136*, 12844.
(28) (a) Mauritz, K. A.; Moore, R. B. *Chem. Rev.* **2004**, *104*, 4535. (b) Orfino, F. P.; Holdcroft, S. *J. New Mater. Electrochem. Syst.* **2000**, *4*, 287.
(29) Agmon, N. *Chem. Phys. Lett.* **1995**, *244*, 456.
(30) (a) Rappé, A. K.; Colwell, K. S.; Casewit, C. J. *Inorg. Chem.* **1993**, *32*, 3438. (b) Rappé, A. K.; Casewit, C. J.; Colwell, K. S.; Goddard, W. a., III; Skiff, W. M. *J. Am. Chem. Soc.* **1992**, *114*, 10024. (c) Casewit, C. J.; Colwell, K. S.; Rappé, A. K. *J. Am. Chem. Soc.* **1992**, *114*, 10035. (d) Casewit, C. J.; Colwell, K. S.; Rappé, A. K. *J. Am. Chem. Soc.* **1992**, *114*, 10046.
(31) Granovsky, A. A. Firefly version 8, http://classic.chem.msu.su/gran/firefly/index.html.
(32) Schmidt, M. W. *J. Comput. Chem.* **1993**, *14*, 1347.

DOI: 10.1021/jacs.5b07267
J. Am. Chem. Soc. 2015, 137, 11498−11506